Hindawi
Advances in Materials Science and Engineering
Volume 2019, Article ID 1376164, 9 pages
https://doi.org/10.1155/2019/1376164

Research Article

Precision Forming Technology for Crimping of Large Straight Welded Pipes

Li-feng Fan,[1] **Pei Liang**,[2] **Ge Wang**,[2] **Ying Gao**,[3] **and Benguo Zhang**[4]

[1]*Transportation Institute, Inner Mongolia University, Hohhot 010070, China*
[2]*National Engineering Research Center for Equipment and Technology of Cold Strip Rolling, Yanshan University, Qinhuangdao 066004, China*
[3]*College of Material Science and Engineering, Hebei University of Science and Technology, Shijiazhuang 050018, China*
[4]*Jiangsu Mould Intelligent Manufacturing Engineering Research Center, Yancheng 224051, China*

Correspondence should be addressed to Li-feng Fan; fanlifeng@imu.edu.cn

Received 5 July 2019; Accepted 14 October 2019; Published 31 October 2019

Guest Editor: Benjamin I. Imasogie

Crimping plays a pivotal role in the production of large-diameter submerged-arc welded pipes. In the crimping forming process, predicting the springback while considering the real-time variation of material parameters is a major challenge faced by many researchers, which has a direct impact on the quality of the welded pipe. To address this problem, the precision forming technology of crimping was developed. The engineering theory of plastic bending was used to investigate the crimping forming process. Two methods, namely, the slope reverse method and the optimization method, were adopted to identify the material parameters. The results showed that the inverted material parameters can be evaluated in real time based on the analytical model of crimping. The maximum relative error of the identification value is less than 4%. Therefore, the springback and displacement during crimping can be predicted dynamically to control the crimping forming quality. Thus, this project provides an important opportunity to achieve precise forming through crimping.

1. Introduction

The forming technology of crimping has been extensively used in the production of large-diameter straight seam submerged-arc welded (LSAW) pipes. To improve the geometry and dimensional accuracy of LSAW pipes, both sides of the sheet edge were bent into a certain nominal curvature by crimping, which can effectively prevent peach breaks and cracking during expansion.

A considerable amount of literature has been published on crimping forming processes. These studies address the stress and strain state of the plate in crimping [1], the effects of technological parameters on the crimping forming quality [2], and the effects of crimping on the pipe quality [3–5] by the finite element analysis (FEA) method.

The most significant disadvantages of FEA in the design of crimping parameters are its time required and the difficulty in identifying material parameters. However, the analytical method can improve the computational efficiency by idealizing the forming conditions. Scholars have analyzed the crimping forming process quality using analytical methods for the design parameters [6, 7], bending moment/forming force [8], stress/strain, and springback [9].

It has previously been observed that the control of springback, which happens after the removal of the forming loads, remains a key issue in the crimping process. A number of intersectional studies have been published on springback calculations [10–12], springback reduction [13, 14], and the springback mechanism [15]. However, few studies have investigated the influence of the fluctuation of mechanical properties on the control accuracy of springback in applications. Hence, efforts have been made to reduce the influence of the fluctuation of mechanical material properties on springback by the robustness design method [16, 17], but this work still has not achieved the purpose of precise forming of crimping.

Therefore, the purpose of this investigation is to propose a precision forming method for crimping. First, the quantitative relationship between the bending displacement and bending force was calculated by the analytical method of crimping. Second, the identification of material parameters was performed by the gray correlation method. Finally, crimping displacement predictions were achieved by the springback prediction model. The ideal crimping displacement can undergo dynamic adjustment by using the precision forming technology for crimping. The proposed technology has demonstrated that it is not only the forming accuracy that can be effectively improved in precision crimping but a lot of design times can be saved.

2. Analytical Model of Crimping

In this study, the analytical method as an efficient tool was used to calculate the quantitative relationship between the bending displacement and bending force. In the crimping forming process, the punch and the edges of the sheet are fixed. With the die loading progressively increasing, the edges of the sheet are gradually bent along the punch surface. Then, the process of unloading the sheet is begun by moving the die down when the sheet reaches the target bending angle. Crimping is completed after springback of the sheet (Figure 1).

The parameter equation of the involute can be used to describe the shape of the punch and die in Cartesian coordinates:

$$\begin{cases} x(\varphi) = R_{\mathrm{p}} \cos\varphi + \varphi R_{\mathrm{p}} \sin\varphi, \\ y(\varphi) = R_{\mathrm{p}} \sin\varphi + \varphi R_{\mathrm{p}} \cos\varphi, \end{cases} \tag{1}$$

where R_{p} is the base radius and φ is the base angle.

To facilitate subsequent calculation, a new XOY coordinate system, with point O as the original point that is the involute end point corresponding to the terminal base angle β_{p}, is established. The parameter equation of the crimping punch in the XOY coordinate system is modified as follows:

$$\begin{cases} X(\varphi) = \left(x(\varphi) - x\left(\beta_{\mathrm{p}}\right)\right)\cos\left(\beta_{\mathrm{p}}\right) + \left(y(\varphi) - y\left(\beta_{\mathrm{p}}\right)\right)\sin\left(\beta_{\mathrm{p}}\right), \\ Y(\varphi) = -\left(x(\varphi) - x\left(\beta_{\mathrm{p}}\right)\right)\sin\left(\beta_{\mathrm{p}}\right) + \left(y(\varphi) - y\left(\beta_{\mathrm{p}}\right)\right)\cos\left(\beta_{\mathrm{p}}\right). \end{cases} \tag{2}$$

Therefore, the curvature radius of punch ρ according to the involute property can be calculated as follows:

$$\rho = R_{\mathrm{p}} \cdot \left(\beta_{\mathrm{p}} - \theta\right), \tag{3}$$

where θ is the crimping bending angle.

In the analytical model of crimping, the description of the material behavior is very important. To simplify the calculation, it is assumed that a state of plane strain exists:

$$\varepsilon = \frac{y}{\rho}. \tag{4}$$

The elastic behavior according to Hooke's law can be written as follows for a state of plane strain:

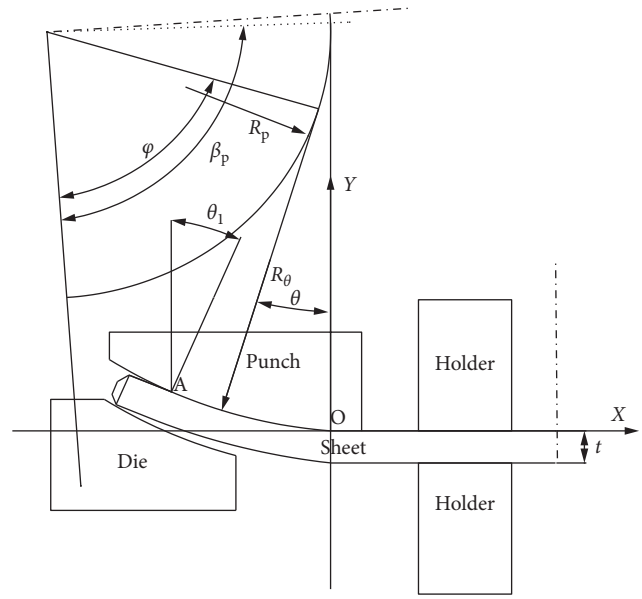

Figure 1: Crimping sketch.

$$\sigma = E\varepsilon. \tag{5}$$

As the stress-strain relationship for plastic deformation, a linear hardening law is adopted here:

$$\sigma = \sigma_{\mathrm{s}} + E_{\mathrm{p}}\varepsilon. \tag{6}$$

In this study, three deformed stages can be determined in the whole crimping forming process: (1) elastic deformation, (2) unwrapped stage in the elastoplastic regime, and (3) wrapped stage in the elastoplastic regime.

2.1. Elastic Deformation Stage. When the radius of curvature in crimping section ρ is larger than the elastic limit radius of curvature ρ_{e}

$$\rho_{\mathrm{e}} = \frac{tE}{2\sigma_{\mathrm{s}}}. \tag{7}$$

In this phase, the crimping deformation occupies the whole elastic deformation stage. Thus, the bending moment can be expressed as

$$M = \frac{EI}{\rho}, \tag{8}$$

where I is the section moment of inertia, $I = 2\int_0^{t/2} y^2 \mathrm{d}y$.

In addition, the bending moment can be calculated according to the external force

$$\begin{cases} M = F_x\left(y_1 - y\right) + F_y\left(x_1 - x\right), \\ F_x = F\sin\theta_1, \\ F_y = F\cos\theta_1, \end{cases} \tag{9}$$

where F_x is the horizontal forming force and F_y is the vertical forming force.

According to the geometry, the following relationships can be obtained:

$$\begin{cases} \dfrac{\mathrm{d}s}{\mathrm{d}\theta} = \rho, \\ \mathrm{d}x = \mathrm{d}s\cos\theta, \\ \mathrm{d}y = \mathrm{d}s\sin\theta. \end{cases} \tag{10}$$

We simultaneously apply equations (8)–(10) and differentiate both sides of the equation:

$$-EI\frac{\mathrm{d}^2\theta}{\mathrm{d}s^2} = F\sin\theta_1\sin\theta + F\cos\theta_1\cos\theta. \tag{11}$$

Note:

$$\frac{\mathrm{d}^2\theta}{\mathrm{d}s^2} = \frac{1}{2}\frac{\mathrm{d}}{\mathrm{d}\theta}\left[\left(\frac{\mathrm{d}\theta}{\mathrm{d}s}\right)^2\right]. \tag{12}$$

Therefore, the equation can become

$$-\frac{EI}{2}d\left[\left(\frac{\mathrm{d}\theta}{\mathrm{d}s}\right)^2\right] = \left(F\sin\theta_1\sin\theta + F\cos\theta_1\cos\theta\right)\mathrm{d}\theta. \tag{13}$$

The following equation can be obtained by integrating both sides of differential equation:

$$-\frac{EI}{2}\left(\frac{\mathrm{d}\theta}{\mathrm{d}s}\right)^2 = -F\sin\theta_1\cos\theta + F\cos\theta_1\sin\theta + C. \tag{14}$$

According to boundary conditions, when $\theta = \theta_1$, $\mathrm{d}s/\mathrm{d}\theta$ and the coefficient $C = 0$. Therefore,

$$\frac{\mathrm{d}s}{\mathrm{d}\theta} = \sqrt{\frac{EI}{2F\left(\sin\theta_1\cos\theta - \cos\theta_1\sin\theta\right)}}. \tag{15}$$

The curve equation can be obtained by solving the differential equation, and the crimping angle θ_1 can be determined by the following formula:

$$s = \int_0^{\theta_1}\psi(\theta)\mathrm{d}\theta = L, \tag{16}$$

where $\psi(\theta) = \sqrt{EI/2F\sin(\theta_1 - \theta)}$.

2.2. Unwrapped Stage in Elastoplastic Deformation. As the bending displacement increases, the bending radius of the curvature is smaller than the maximum elastic radius of the curvature but still larger than the radius of curvature of the punch. The stage enters the unwrapped stage in elastoplastic deformation. Therefore, the entire deformation section can be divided into an elastic deformation section and an elastic-plastic deformation section. The elastic-plastic bending moment M can be expressed as

$$M = A\rho^2 + B\frac{1}{\rho} + C, \tag{17}$$

where $A = ((2\sigma_s^3 - 2E_p\sigma_s^3)/3E^2) - (\sigma_s^3/E^2)(1 - (E_p/E))$, $B = E_p t^3/12$, and $C = (\sigma_s t^4/4)(1 - (E_p/E))$.

The differential equations can be obtained by simultaneous application of equations (2) and (3):

$$A\left(\frac{\mathrm{d}s}{\mathrm{d}\theta}\right)^2 + B\left(\frac{\mathrm{d}\theta}{\mathrm{d}s}\right) + C = F_x(y_1 - y) + F_y(x_1 - x). \tag{18}$$

Differentiate as follows:

$$A\frac{\mathrm{d}}{\mathrm{d}s}\left[\left(\frac{\mathrm{d}s}{\mathrm{d}\theta}\right)^2\right] + B\frac{\mathrm{d}}{\mathrm{d}s}\left(\frac{\mathrm{d}\theta}{\mathrm{d}s}\right) = -F_x\frac{\mathrm{d}y}{\mathrm{d}s} - F_y\frac{\mathrm{d}x}{\mathrm{d}s}. \tag{19}$$

Note that

$$2\frac{\mathrm{d}^2s}{\mathrm{d}\theta^2} = \frac{\mathrm{d}}{\mathrm{d}s}\left[\left(\frac{\mathrm{d}s}{\mathrm{d}\theta}\right)^2\right]. \tag{20}$$

The differential equation can be obtained as follows:

$$2A\frac{\mathrm{d}^2s}{\mathrm{d}\theta^2} + B\frac{\mathrm{d}^2\theta}{\mathrm{d}s^2} = -F\cos(\theta_1 - \theta). \tag{21}$$

The conditions $\theta = \theta_p$ and $s = l_p$ mark the boundary point between the elastic section and the elastoplastic section. In addition, at $M = M_{\max-e}$, the following formula can be satisfied:

$$M_{\max-e} = \sqrt{2FEI\sin\left(\theta_1 - \theta_p\right)} = \frac{1}{6}\sigma_s t^2. \tag{22}$$

From this boundary condition, the relationship between F and the position of the boundary point is given but depends only on the value that cannot be determined by the elastoplastic deformation section, and the elastic deformation section is needed to supplement the solution:

$$s = \int_{\theta_p}^{\theta_1}\psi(\theta)\mathrm{d}\theta = L - l_p = l_e. \tag{23}$$

2.3. Elastoplastic Deformation Wrapped Stage. As the bending deformation increases, the radius of curvature becomes equal to the radius of curvature of the punch at the corresponding position, and the deformation is in the elastoplastic deformation wrapped stage. The whole sheet can be divided into three sections: elastic, elastoplastic unwrapped, and elastoplastic wrapped section.

The relationship between the bending moment and the curvature of the elastic-plastic cladding section can be calculated according to the radius of curvature of the convex model surface. The origin of the coordinate system is translated to the centroid of the starting position of the bending of the sheet, and the downward translation is available:

$$\begin{cases} x^*(\varphi) = \left[x(\varphi) - x\left(\beta_p\right)\right]\cos\beta_p + \left[y(\varphi) - y\left(\beta_p\right)\right]\sin\beta_p, \\ y^*(\varphi) - \left[x(\varphi) - x\left(\beta_p\right)\right]\sin\beta_p + \left[y(\varphi) - y\left(\beta_p\right)\right]\cos\beta_p + \dfrac{t}{2}. \end{cases} \tag{24}$$

According to the involute property, the curvature radius of the sheet intermediate layer ρ_θ can be known:

$$\rho_\theta = R_p\cdot\left(\beta_p - \theta\right) + \frac{t}{2}. \tag{25}$$

Therefore, the bending moment of the covered section is

$$M_\theta = \left[\frac{2\sigma_s^3 - 2E_p\sigma_s^3}{3E^2} - \frac{\sigma_s^3}{E^2}\left(1 - \frac{E_p}{E}\right)\right]\rho_\theta^2 + \frac{E_p t^3}{12}\frac{1}{\rho_\theta} + \frac{\sigma_s t^4}{4}\left(1 - \frac{E_p}{E}\right). \tag{26}$$

According to the involute arc length formula, the length of the wrapping section can be obtained as

$$l_w = \int_\theta^{\theta_w} \sqrt{\left(\frac{dx^*}{d\theta}\right)^2 + \left(\frac{dy^*}{d\theta}\right)^2}\, d\theta. \tag{27}$$

When $\theta_w \le \theta \le \theta_p$, the length of the unwrapping section can be obtained from

$$2A\frac{d^2 s}{d\theta^2} + B\frac{d^2\theta}{ds^2} = -F\cos(\theta_1 - \theta). \tag{28}$$

The elastic deformation section is needed to supplement the solution:

$$s = \int_{\theta_p}^{\theta_1} \psi(\theta) d\theta = L - l_p - l_w. \tag{29}$$

2.4. Verification for Analytical Model. In this study, an X80 grade Φ1219 × 22 × 12000 mm large-diameter straight seam welded pipe was taken as an example, and a #3 crimping mold was adopted as the research object. The mold parameters are shown in Table 1.

To evaluate the precision of the bending analysis model, the crimping forming process was conducted by a hydropress in the plant. The forming force and displacement can be collected with a pressure sensor and a displacement sensor. Then, the comparison between the measured values and those calculated from the analytical model is shown in Figure 2.

As seen from Figure 2, the calculation results are in good agreement with the measurement results and their maximum relative error is less than 9.06%.

3. Identification of the Material Parameters

To adjust the forming parameters online, it is necessary to identify the mechanical properties of materials in real time considering the influence of fluctuations of the mechanical material properties on the springback. Therefore, first, the effects of the mechanical properties on the bending load curve are analyzed based on the crimping analytical model, and then the initial segment of the bending load curve is used to identify the elastic modulus. Finally, the objective function is constructed by the gray correlation method, and the yield strength and the plastic modulus are identified by the inverse optimization method. In this section, the #3 crimping mold remains the research object.

3.1. Effects of the Material Parameters on the Forming Force. To improve the identification accuracy and efficiency, the effects of the elastic modulus, yield strength, and plastic modulus on the bending displacement and bending load curve are analyzed, as shown in Figures 3–6.

Table 1: Parameters of the crimping mold.

Parameters	Value
Base radius of punch R_p (mm)	303.20
Terminal angle of the punch β_p (°)	88
Base radius of the die R_d (mm)	303.20
Terminal angle of the die β_d (°)	88
Length of crimping B (mm)	190
Horizontal distance between the punch and die D (mm)	80

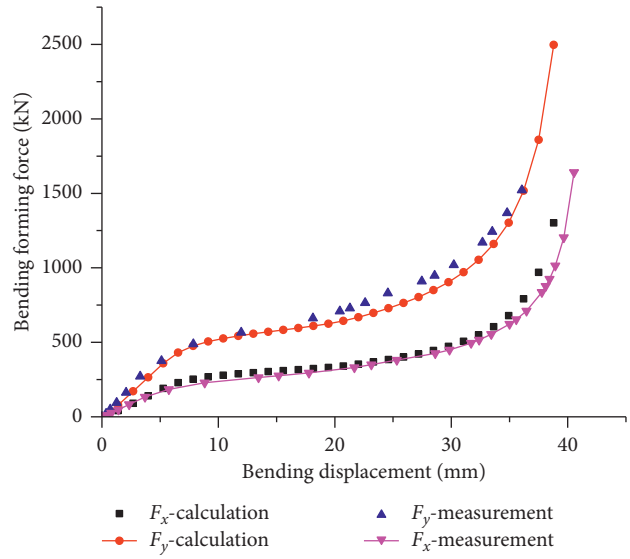

Figure 2: Verification with bending force.

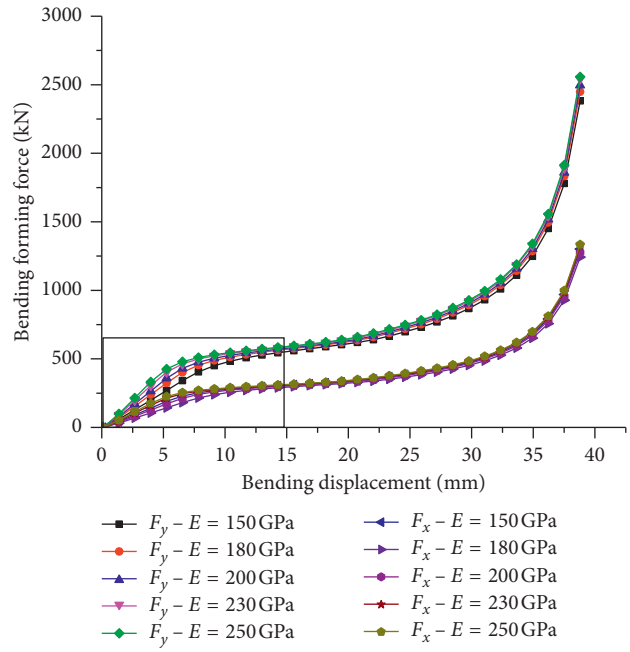

Figure 3: Effects of the elastic modulus on the bending load.

It can be seen from Figures 3 and 4 that the elastic modulus has a significant influence on the initial segment of the curve and has little effect on the subsequent plastic

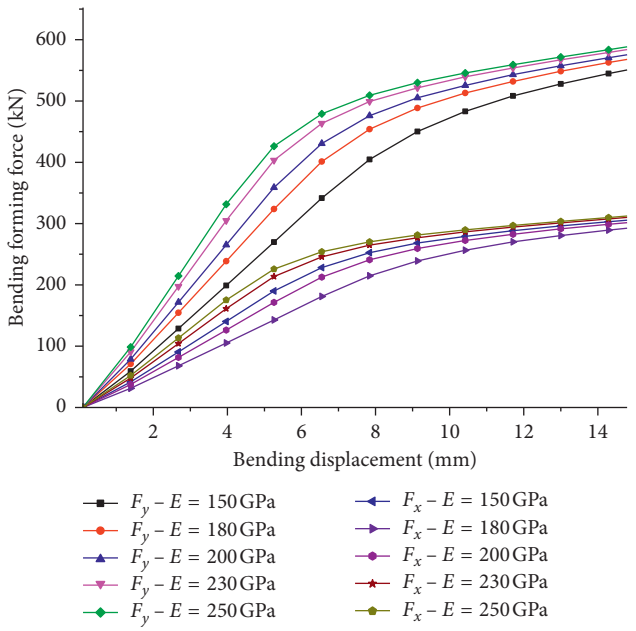

Figure 4: Partial enlargement of Figure 3.

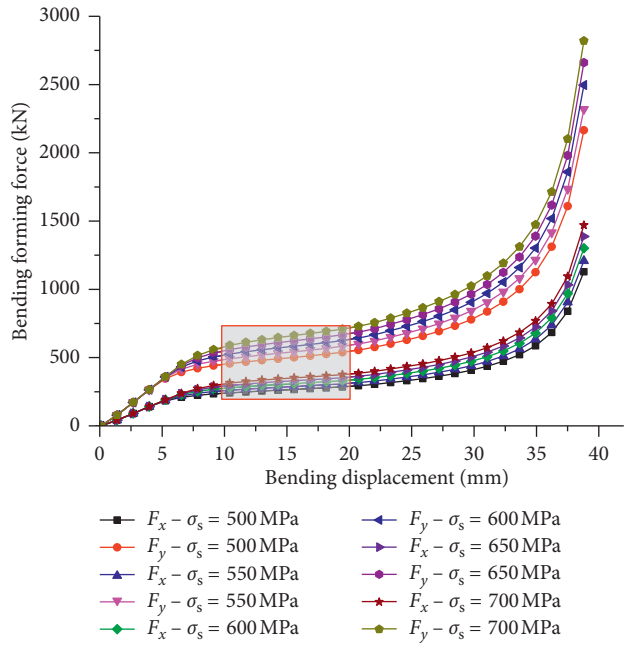

Figure 5: Effects of the yield strength on the bending load.

segment, and it is found that the initial segment of the curve is approximately linear.

It can be seen from Figures 5–8 that the change of the yield strength has no effect on the initial section of the curve, but the influence on the subsequent plastic section of the curve is more obvious, and the bending load increases as the yield strength increases with the same bending stroke.

3.2. Identification of the Elastic Modulus. In the elastic deformation stage, it was determined from the theoretical

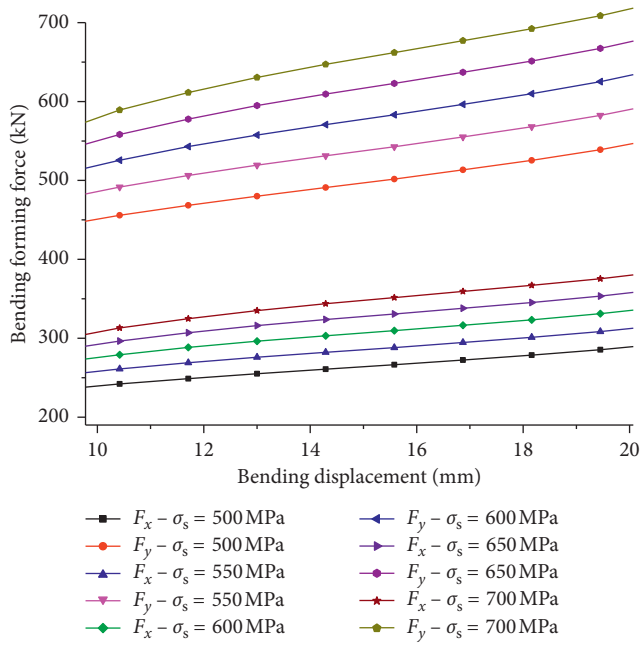

Figure 6: Partial enlargement of Figure 5.

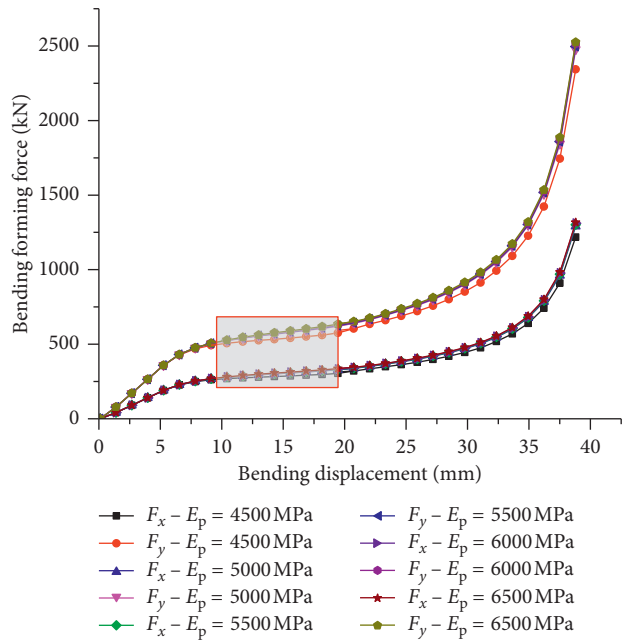

Figure 7: Effects of the plastic modulus on the bending load.

analytical model that only the elastic modulus has a direct influence on the bending load. The analysis of the influence rate of the elastic modulus on the forming load at different displacements is shown in Figure 9. This demonstrated that in the elastic deformation stage ($h < 5$ mm), the degree of influence increases with increasing displacement and that linearity is satisfied.

However, in the plastic deformation stage, the plastic material parameters play a major role, and the influence of the elastic modulus on the forming load is weakened. To

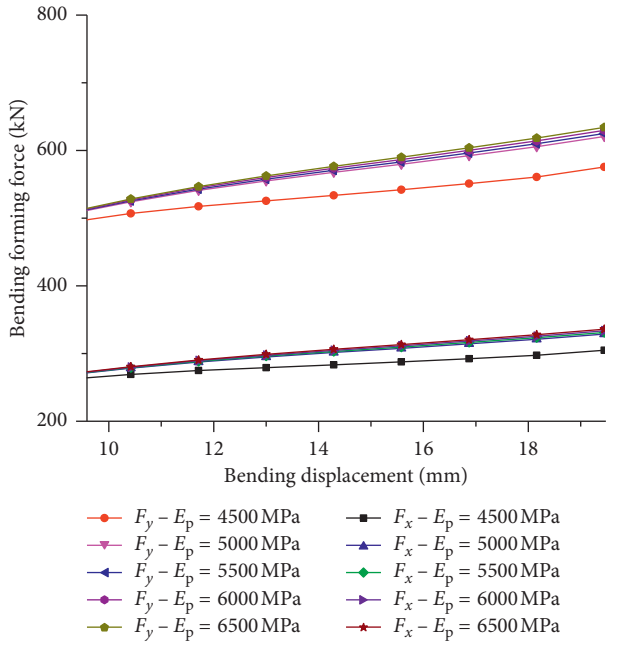

Figure 8: Partial enlargement of Figure 7.

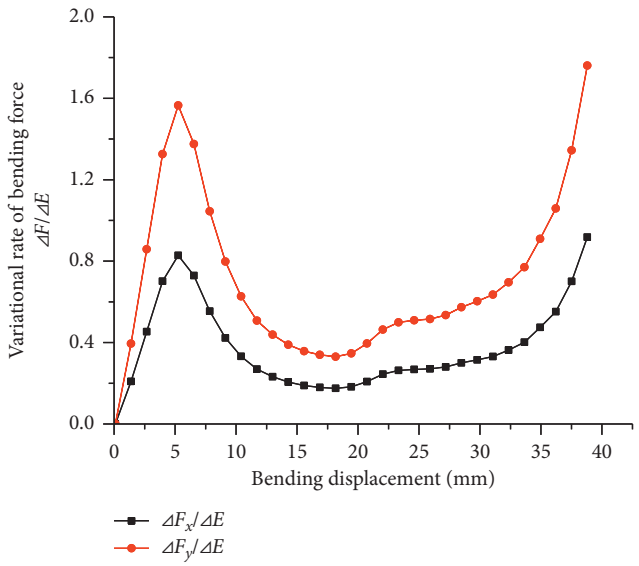

Figure 9: Effect of the rate elastic modulus on the bending load.

identify the elastic modulus in the elastic deformation stage, the effect of the elastic modulus on the slope of the loading curve at the elastic deformation stage is analyzed in Figure 10, as fit by the following linear formula:

$$\begin{cases} E = -0.0028S_y + 402.07, \\ E = -0.0053S_x + 402.08, \end{cases} \quad (30)$$

where E is the elastic modulus and S_x, S_y is the slope of the horizontal and vertical forming forces, respectively.

Therefore, the elastic modulus can be identified by equation (30).

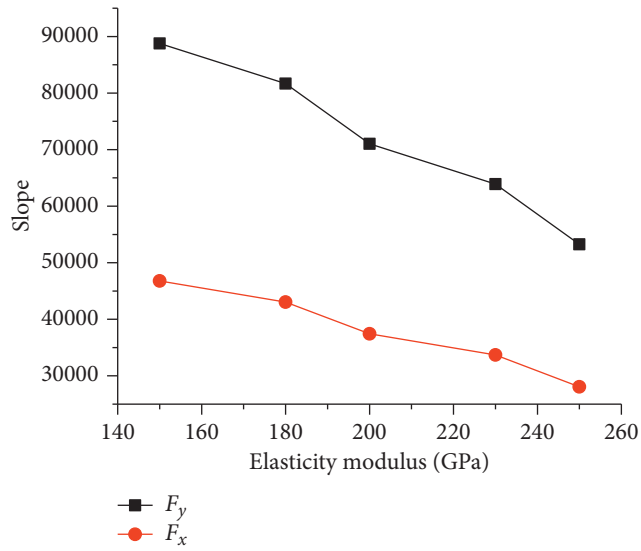

Figure 10: Effects of the elastic modulus on the slope of the loading curve during the elastic deformation stage.

3.3. Plastic Parameter Inversion. It is found that both the yield strength and the plastic modulus have a significant influence on the plastic segment of the bending load curve, and its trends are to increase slowly and then rapidly in Figures 11 and 12.

Therefore, to identify the plastic parameters, the yield strength and plastic modulus are substituted into the crimping analytical model for trial calculation by the optimization algorithm, in which the calculated curve is refined to approximate the measured curve until it reaches the allowable error.

The gray relational theory was applied to construct the objective function of inverse identification f_{object}, which can comprehensively evaluate the approximation characteristics of the calculated curve and the measured curve as follows.

3.3.1. Reference Sequence and Relative Sequence. The bending loads $F^e = [F_1 \ F_2 \ \dots \ F_n]$ corresponding to the measured bending displacements $h = [h_1 \ h_2 \ \dots \ h_n]$ were selected as the reference sequence, and then the bending loads $F_i(k) = [F_i(1) \ F_i(2) \ \dots \ F_i(n)]$ corresponding to the bending displacements $h = [h_1 \ h_2 \ \dots \ h_n]$ were calculated by the analytical model by a genetic algorithm for comparison.

3.3.2. Dimensionless Data. To facilitate analysis, it is necessary to conduct dimensionless data processing on the original data before the comparison. When the target has visual characteristics, the data processing is as follows:

$$F_i^d(k) = \frac{F_i(k) - \min\limits_{i \in N} F_i(k)}{\max\limits_{i \in N} \left|F_i(k) - F^e(k)\right| - \min\limits_{i \in N} \left|F_i(k) - F^e(k)\right|}, \quad (31)$$

where $F_i^d(k)$ is the $F_i(k)$ data processing results.

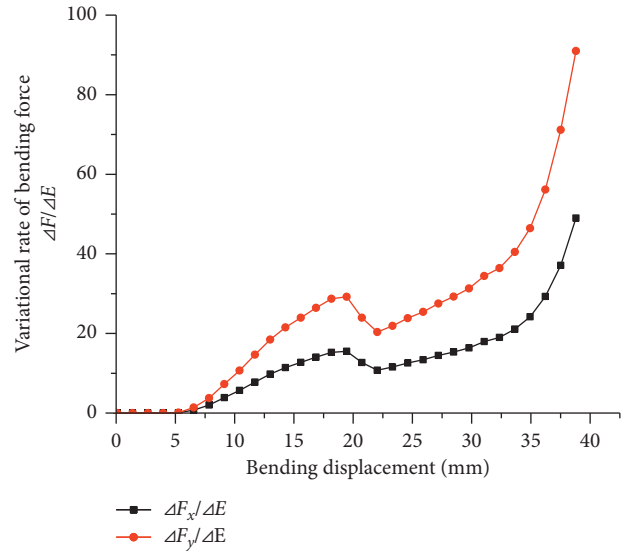

Figure 11: Effect of the rate plastic modulus on the bending load.

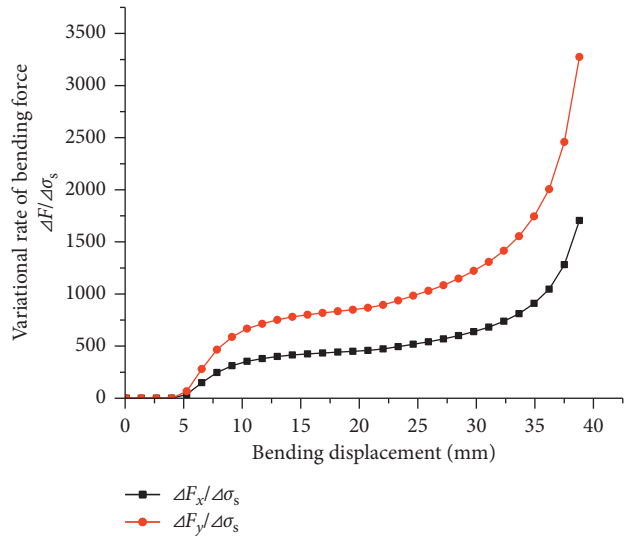

Figure 12: Effect of the rate yield strength on the bending load.

3.3.3. Gray Correlation Coefficient. The gray relational coefficients were used to measure the difference between the theoretical and experimental results. The gray relational coefficient $\xi_i(k)$ can be written as follows:

$$\xi_i(k) = \frac{\min\limits_{i\in N}\min\limits_{i\in N}\left|F^e(k) - F_i(k)\right| + \rho\max\limits_{i\in N}\max\limits_{i\in N}\left|F^e(k) - F_i(k)\right|}{\left|F^e(k) - F_i(k)\right| + \rho\max\limits_{i\in N}\max\limits_{i\in N}\left|F^e(k) - F_i(k)\right|}, \quad (32)$$

where $\rho = 0.5436$.

3.3.4. Gray Relational Grade. The gray relational grade corresponding to each performance characteristic is computed, and the overall evaluation of the multiresponse characteristics is based on the gray relational grade, which is given by [18]:

$$r(F^e, F_i) = \frac{1}{n}\sum_{k=1}^{n}\lambda_k\xi_i(k). \quad (33)$$

A higher gray relational grade represents that the experimental result is closer to the ideally normalized value.

3.3.5. Gray Difference Degree. In the optimization design, the minimum value of the objective function is usually obtained, so the concept of gray difference degree is introduced [19]:

$$d_i = 1 - r(F^e, F_i). \quad (34)$$

Therefore, the above gray difference is used as the objective function of identification optimization:

$$f_{\text{object}} = \min\left[d_i(F^e, F_i)\right]. \quad (35)$$

Finally, the optimization model is constructed as follows:

$$\begin{aligned} &\text{design variable}\left(\sigma_s, E_p\right),\\ &\text{constraint condition}\begin{cases}\sigma_s^l \le \sigma_s \le \sigma_s^u,\\ E_p^l \le E_p \le E_p^u,\end{cases}\\ &f_{\text{object}} = \min\left[d_i(F^e, F_i)\right]. \end{aligned} \quad (36)$$

The relatively stable NLPQL (nonlinear programming by quadratic Lagrangian) algorithm is selected as the inversion optimization algorithm to solve the optimization model, which expands the objective function by the second-order Taylor series, linearizes the constraint condition, and obtains the next design point by solving the quadratic programming optimization problem. Finally, the plastic parameters, including the yield strength and plastic modulus, were identified by optimization.

3.4. Verification for Parameter Identification. To verify the reliability of the parameter identification technology, the material mechanical properties of X80 were calculated by the parameter identification technique described in 3.3 and compared with the results of the uniaxial tensile test in Table 2.

As seen from Table 2, the maximum relative error of the identification value is less than 4%. This satisfies the requirements.

4. Crimping Displacement Prediction

4.1. Springback Prediction Model. To predict the crimping displacement, a calculation model of the springback must be constructed by the analysis method. Thus, according to unloading laws, the curvature after springback can be obtained by

$$\frac{1}{\rho_\theta'} = \frac{1}{\rho_\theta} - \frac{1}{\rho_\theta^e}. \quad (37)$$

The springback curvature can be expressed as follows:

Table 2: Comparison with identification and test.

Parameters	Identification	Test	Relative error (%)
Elastic modulus E (GPa)	203	210	3.3
Yield strength σ_s (MPa)	575	596	3.5
Plastic modulus E_p (MPa)	5702	5500	3.67

$$\frac{1}{\rho_\theta^e} = \frac{M_\theta}{EI}. \tag{38}$$

For the elastoplastic deformation wrapped stage, the bending moment can be calculated by equations (25) and (26). For the unwrapped stage in elastoplastic deformation, the bending moment can be calculated by equation (16). In addition, the differential equations can be established:

$$\frac{1}{\rho_\theta'} = \frac{ds}{d\theta}. \tag{39}$$

When $M = M_{\max-e} = (1/6)\sigma_s t^2$, $\theta = \theta_p$, and $s = l_p$, the angle after springback $\theta = \theta_*$ can be obtained by solving the above differential equations. Then, we evaluate whether the crimping angle after springback satisfies the target value, and if this condition is satisfied, the predicted displacement is obtained. If not, the displacement is increased and recalculated until the criterion is satisfied.

To evaluate the precision of the springback analysis model, the crimping forming process is conducted by a hydropress in the plant. The forming force and displacement can be collected with a pressure sensor and a displacement sensor. Then, the comparison between measurement and calculation from the analytical model is shown in Figure 13.

As seen from Figure 13, the calculation results are in good agreement with the measurement results and their maximum relative error is 4.76%.

4.2. Application. In this study, a $\Phi 1219 \times 22 \times 12000$ mm large-diameter straight seam welded pipe was taken as an example. First, the elastic modulus E, yield strength σ_s, and plastic modulus E_p of the mechanical properties of the material were determined by tensile testing. Then, a #3 mold was used for crimping forming.

To verify the feasibility of precision forming technology for crimping, the crimping forming process was performed using different displacements: 23, 28, 33, 38, and 42 mm. The forming displacement can be obtained from the displacement sensor, and the crimping angle after springback was measured by three-coordinate measuring instruments. Finally, a comparison between the calculations and measurements is shown in Figure 14.

It can be seen from Figure 14 that the proposed precise forming technology can dynamically adjust the bending displacement in real time and effectively control the quality of crimping forming.

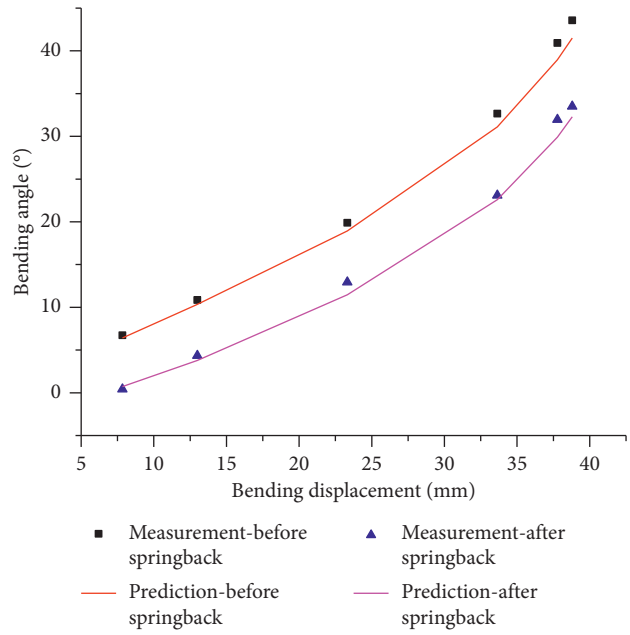

Figure 13: Verification with the bending angle.

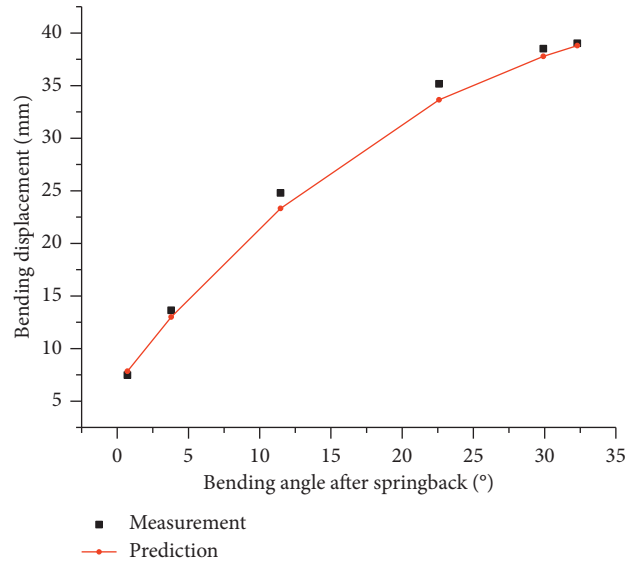

Figure 14: Verification with bending angle and bending displacement.

5. Conclusions

To calculate the springback considering the real-time variation of material parameters, the identification of material parameters was performed by an analytical model of crimping and the inverse optimization method. Then, the crimping displacement was predicted based on the springback model. The conclusions were as follows:

(1) Three phases compose the whole crimping forming process: the elastic deformation stage, the unwrapped stage in elastoplastic deformation, and the wrapped stage in elastoplastic deformation. The

quantitative relationship between the bending displacement and bending force was calculated by an analytical model of crimping.

(2) The elastic modulus has a significant effect on the bending force curve, and the initial segment of the bending force curve is approximately linear. The elastic modulus can be identified by the linear formula.

(3) The yield strength and the plastic modulus have a significant effect on the plastic segment of the bending load curve, and the trends are to increase slowly and then rapidly. The plastic parameters, including the yield strength and plastic modulus, can be identified by the gray correlation method.

(4) Precision forming technology for crimping was achieved by identification of the material parameters and by crimping displacement prediction technology.

Data Availability

The datasets supporting the conclusions of this article are included within the article.

Conflicts of Interest

The authors declare no conflicts of interest.

Authors' Contributions

Li-Feng Fan supervised the research and wrote the manuscript and the others assisted with sampling and laboratory analyses.

Acknowledgments

The authors thank Professor Ying Gao of Hebei University of Science and Technology for his critical discussion and reading during manuscript preparation. This study was supported by the National Natural Science Foundation of China (51761030) and the Inner Mongolia Natural Science Foundation of China (2019MS05081).

References

[1] G. Palumbo and L. Tricarico, "Effect of forming and calibration operations on the final shape of large diameter welded tubes," *Journal of Materials Processing Technology*, vol. 164-165, no. 5, pp. 1089–1098, 2005.

[2] L. Fan, Y. Gao, Q. Li, and H. Xu, "Quality control on crimping of large diameter welding pipe," *Chinese Journal of Mechanical Engineering*, vol. 25, no. 6, pp. 1264–1273, 2012.

[3] J. Liu, K. Huang, and F. Ruan, "Effects of the parameters of prebending on O-forming of pipe in UOE process," *Journal of Plasticity Engineering*, vol. 12, no. 3, pp. 71–75, 2005, in Chinese.

[4] M. D. Herynk, S. Kyriakides, A. Onoufriou, and H. D. Yun, "Effects of the UOE/UOC pipe manufacturing processes on pipe collapse pressure," *International Journal of Mechanical Sciences*, vol. 49, no. 5, pp. 533–553, 2007.

[5] T. Zou, G. Wu, D. Li, Q. Ren, J. Xin, and Y. Peng, "A numerical method for predicting O-forming gap in UOE pipe manufacturing," *International Journal of Mechanical Sciences*, vol. 98, no. 5, pp. 39–58, 2015.

[6] L. Hong, "Prebending process of longitudinal submerged arc welding production line," *Welding Pipe and Tube*, vol. 29, no. 1, pp. 55–57, 2006, in Chinese.

[7] Z. Xie and J. Xia, "Prebending process parameter design of longitudinal submerged arc welding pipe," *Welding Pipe and Tube*, vol. 30, no. 3, pp. 52–54, 2007, in Chinese.

[8] S. Zhao, *Study on Quality Control Strategy and Simulation System Development of UOE Pipe Forming*, Yanshan University, Qinhuangdao, China, 2010, in Chinese.

[9] Q. Yang, *Springback Analytic and Process Parameters Optimization of Plate Edge Preflex for the Forming of Large Diameter Longitudinal Seam Welded pipe*, Yanshan university, Qinhuangdao, China, 2012, in Chinese.

[10] P.-A. Eggertsen and K. Mattiasson, "On constitutive modeling for springback analysis," *International Journal of Mechanical Sciences*, vol. 52, no. 6, pp. 804–818, 2010.

[11] S. Sumikawa, A. Ishiwatari, J. Hiramoto, and T. Urabe, "Improvement of springback prediction accuracy using material model considering elastoplastic anisotropy and Bauschinger effect," *Journal of Materials Processing Technology*, vol. 230, pp. 1–7, 2016.

[12] W. Julsri, S. Suranuntchai, and V. Uthaisangsuk, "Study of springback effect of AHS steels using a microstructure based modeling," *International Journal of Mechanical Sciences*, vol. 135, pp. 499–516, 2018.

[13] L. Komgrit, H. Hamasaki, R. Hino, and F. Yoshida, "Elimination of springback of high-strength steel sheet by using additional bending with counter punch," *Journal of Materials Processing Technology*, vol. 229, pp. 199–206, 2016.

[14] Z. Wang, Q. Hu, J. Yan, and J. Chen, "Springback prediction and compensation for the third generation of UHSS stamping based on a new kinematic hardening model and inertia relief approach," *The International Journal of Advanced Manufacturing Technology*, vol. 90, no. 1–4, pp. 875–885, 2017.

[15] J. H. Kim, D. Kim, F. Barlat, and M.-G. Lee, "Crystal plasticity approach for predicting the Bauschinger effect in dual-phase steels," *Materials Science and Engineering: A*, vol. 539, pp. 259–270, 2012.

[16] L. Fan, Y. Gao, Q. Li, and H. Xu, "Designing for robustness on crimping of large diameter welding pipe," *China Mechanical Engineering*, vol. 26, no. 8, pp. 1112–1116, 2015, in Chinese.

[17] J. Yan, L. Fan, and J. Yun, "Stochastic analysis of crimping quality of large diameter welding pipe," *Mechanical Science and Technology for Aerospace Engineering*, vol. 34, no. 12, pp. 1880–1884, 2015, in Chinese.

[18] S. Yarmohammadisatri, M. H. Shojaeefard, A. Khalkhali, and S. Goodarzian, "Sensitivity analysis and optimization of suspension bushing using Taguchi method and grey relational analysis," *International Journal of Vehicle Mechanics and Mobility*, vol. 57, no. 6, pp. 855–873, 2019.

[19] A. B. Shinde and P. M. Pawar, "Multi-objective optimization of surface textured journal bearing by Taguchi based grey relational analysis," *Tribology International*, vol. 114, pp. 349–357, 2017.